ACS APPLIED ELECTRONIC MATERIALS

pubs.acs.org/acsaelm Article

Radio-Frequency Characteristics of Ge-Doped Vanadium Dioxide Thin Films with Increased Transition Temperature

Andrei Muller,* Riyaz A. Khadar, Tobias Abel, Nour Negm, Teodor Rosca, Anna Krammer, Matteo Cavalieri, Andreas Schueler, Fatemeh Qaderi, Jens Bolten, Max Lemme, Igor Stolichnov, and Adrian M. Ionescu*

Cite This: https://dx.doi.org/10.1021/acsaelm.0c00078 Read Online

ACCESS | Metrics & More | Article Recommendations

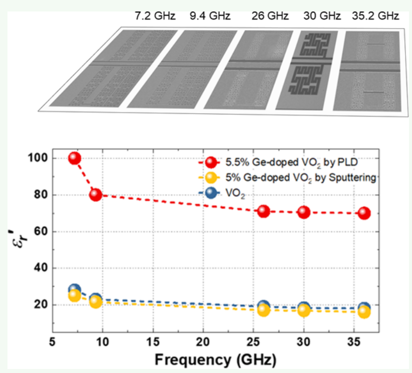

ABSTRACT: This work investigates and reports on the radio-frequency (rf) behavior in the frequency range of 5−35 GHz of germanium-doped vanadium dioxide (Ge-doped VO_2) thin films deposited on silicon substrates via sputtering and pulsed laser deposition (PLD) with estimated Ge concentrations of 5 and 5.5%. Both films exhibit critical transition temperatures (T_c) of 76.2 and 72 °C, respectively, which are higher compared to that of the undoped VO_2 which undergoes reversible insulator-to-metal phase transition at 68 °C. Both types of Ge-doped films show low hysteresis (<5 °C) in their conductivity versus temperature characteristics and preserve high off-state dc-conductivities (corresponding to the insulating state of the phase change material) of 13 S/m for the sputtered and 55 S/m for the PLD-deposited film, respectively. The dc on-state (corresponding to the conductive state of the phase change material) conductivity reaches 145,000 S/m in the case of the PLD film, which represents a significant increase compared to the state-of-the art values measured for undoped VO_2 thin films deposited on identical substrates. In order to further understand the off-state dissimilarities and rf behavior of the deposited Ge-doped VO_2 films, we propose an original methodology for the experimental extraction of the dielectric constant (ε_r) in the GHz range of the films below 60 °C. This is achieved by exploiting the frequency shift of resonant filters. For this purpose, we have fabricated coplanar waveguide structures incorporating ultracompact Peano space-filling curves, each resonating at a different frequency between 5 and 35 GHz on two types of substrates, one with the Ge-doped VO_2 thin films and another one using only SiO_2 to serve as the reference. The reported results and analysis contribute to the advancement of the field of metal−insulator−transition-material technology with high T_c for rf industrial applications.

KEYWORDS: *phase change materials, radio frequency passive circuits, vanadium dioxide, dielectric constant, coplanar waveguide, CMOS, lossy dielectrics*

1. INTRODUCTION

Recently, the applications of Mott insulators showing metal-to-insulator transitions have been actively explored,[1−3] as the phase transitions could be triggered facts, practically in sub-nanosecond timescales and also because the device operation can be done purely electrically, with technologies compatible with silicon complementary metal oxide semiconductor (CMOS). The key feature of Mott insulators is related to the fact that the energy of many other interactions is on the same order of magnitude with electron−electron correlation and kinetic energy; as a consequence, such interactions could play a relevant role on the electronic properties of the material. The phase-change material, vanadium dioxide (VO_2,) exhibits a monoclinic crystal structure and behaves like an insulator below its insulating-to-metal transition temperature (T_{ITM}). Subject of many controversies, it is currently agreed that the phase transition in VO_2 is probably a combined effect of lattice distortion and Coulomb correlations. Because of its ease of integration, reversible insulator to metal transition (IMT), fast switching time, and device-size shrinking capabilities, the employment of VO_2 as a reconfigurable radio-frequency (rf) material has been recently investigated for a variety of rf-reconfigurable devices on various substrates such as sapphire,[4−8] or cheaper SiO_2[9−16] among others, in the frequency (f) range of 1−35 GHz. The relatively low transition temperature of VO_2 of T_c = 68 °C when deposited on silicon (Si) CMOS compatible substrates hinders its usability for developing rf switches because for most rf applications, it is

Received: January 31, 2020
Accepted: April 16, 2020
Published: April 16, 2020

Table 1. Overview of the Dielectric Loss Modeling of VO_2 Thin Films in the Off-State at Different Frequency Bands

references	frequency spectrum	dielectric constant $\varepsilon'_{r,VO_2}(f)$	conductivity $\sigma_{ac\_OFF}(f)$	model, simulation, and assumptions
1, 3 5, 8,	rf		$\sigma_{OFF}(f) = \sigma_{dc\_OFF}$	•simulated as a resistive material •area occupied by VO_2 is very small compared to the device area
9	rf		$\sigma_{OFF}(f) = \sigma_{dc\_OFF}$	•same as above
10,13	rf	30	$\sigma(f_0) = \sigma_{dc\_OFF}$	•simulated as a non-causal dielectric violating Kramers−Kronig relations on SiO_2−Si substrates •area occupied by VO_2 is very small compared to the device area
4	rf	$\varepsilon'_{r,VO_2}(f)$	yes from $\varepsilon''_{r,VO_2}(f)$	•on sapphire •extracted via conformal mapping, assuming infinite ground planes, simplified lossesmodel[37]
18,24	optical	$\varepsilon'_{r,VO_2}(f)$	yes from $\varepsilon''_{r,VO_2}(f)$	•obeying Kramers−Kronig relations via different models (Lorentz, Tauc−Lorentz, etc.)

required to have a switching temperature above 80 °C.[17] On the other hand, the dc conductivity levels of VO_2 thin films in their insulating off-state (σ_{dc_OFF}) and conductive on-state (σ_{dc_ON}) vary over a wide range depending on the substrates used for deposition and hence the built-in lattice mismatches.[18] Doping VO_2 proved to be a solution for changing the critical transition temperature, T_c (which is defined as the average between the T_{ITM} and the metal-to-insulator transition temperature T_{MIT}). This shift was downward while doping with Co on Al_2O_3 substrates[19] or upward to T_c = 93.6 °C using Ge on Si-substrates as shown in our previous work;[20] however, the conductivity level, σ_{dc_ON} obtained above 93.6 °C was below 360 S/m (for Ge concentrations of 5.9%), which is far lower than σ_{dc_ON} obtained for undoped VO_2 (which are higher than 10,000 S/m) when the latter was employed for rf research applications.[13−16]

Unlike the range of optical frequencies, where ellipsometry (a far-field approach) is a powerful tool for the determination of the relative dielectric permittivity of the VO_2, given by

$$\varepsilon_{r,VO_2}(f, T) = \varepsilon'_{r,VO_2}(f, T) + j\varepsilon''_{r,VO_2}(f, T) \quad (1)$$

when thin films are deposited on different substrates,[21−27] near-field approach or conformal mapping[7] are used in rf engineering of electronic functions.

In the rf range, to the best of our knowledge, no study is available in the literature about the dielectric constant, ($\varepsilon'_{r,VO_2:Ge}(f, T)$), of Ge-doped VO_2 deposited on CMOS compatible substrates or its relative dielectric permittivity

$$\varepsilon_{r,VO_2:Ge}(f, T) = \varepsilon'_{r,VO_2:Ge}(f, T) + j\varepsilon''_{r,VO_2:Ge}(f, T) \quad (2)$$

Even for undoped VO_2, models used within 1−30 GHz for the relative dielectric function are in their incipient stages of development and exist only for the case of a VO_2 thin film on a sapphire substrate obtained by using conformal mapping approximations.[7]

In most cases, for the modeling of the off-state conductivity in rf VO_2 thin films used for switches, the authors usually consider the material as a constant valued sheet resistance while seldom simulating it as a lossy dielectric, as depicted in Table 1. The conductivity, σ_{dc_OFF} values measured at room temperature are then assumed as representative for the whole range of rf performances ($\sigma_{ac}(f) = \sigma_{dc\_OFF}$), and VO_2 is modeled as sheet resistance or resistance.[4−12] On the other hand, for thin VO_2 films deposited on SiO_2−Si CMOS compatible substrates, these films are simulated as a lossy dielectric,[13−16] the σ_{dc_OFF} being considered as the conductivity value at the central frequency (f_0) of the analyzed frequency band of the simulations ($\sigma_{ac}(f_0) = \sigma_{dc\_OFF}$), whereas a fixed empirical value of 30 is used for the dielectric constant, ε'_{rVO_2} of VO_2 at room temperature.

The 3D electromagnetic field simulation software—Ansys HFSS (v. 17.2), used for modeling in rf applications[13−16,28,29] has three predefined different models, two of which are based on the Debye model and one other based on the Djordjevic−Sarkar frequency dispersion model.[30,31] Their use avoids improper definition of the material,[32] the latter one being used by default when losses exceed certain limits[33] (unless deactivated by the user). When using one of these existing frequency dispersive models, the Kramers−Kronig relations followed by all real and imaginary parts of the dielectric functions of any causal material[34] are obeyed, but only according to these particular models. Conversely, using the simplified models in[13−16] (where authors use VO_2 only on a limited area of the devices) and assuming a constant $\varepsilon'_{rVO_2}(f, T = 25\,°C)$ and a nonconstant $\varepsilon''_{r,VO_2}(f, T = 25\,°C) = \frac{\sigma_{ac}(f, T = 25\,°C)}{2\pi f\varepsilon_0}$[7,35] (where ε_0 denotes the vacuum permittivity) violates the Kramers−Kronig relations because a frequency-independent dielectric constant implies a constant imaginary part, and this is obeyed only by vacuum.[34]

In this work, we first do a dc characterization of two germanium-doped VO_2 films with doping concentrations of 5 and 5.5% prepared via sputtering and pulsed laser deposition (PLD), respectively, on CMOS-compatible SiO_2/high-resistivity silicon substrates. We compare their temperature-dependent dc conductivity levels, $\sigma_{dc}(T)$ and temperature hysteresis (defined as $T_{ITM} - T_{MIT}$) with other undoped VO_2 depositions done in similar conditions by us.[16] The PLD (243 nm) and sputtered (183 nm) Ge-doped VO_2 films exhibit T_c's of 72 and 76.2 °C, respectively, and present σ_{dc_ON} values which are orders of magnitude higher than that of the 5.9% Ge-doped VO_2 thin film from our previous work[20] with T_c = 93.6 °C.

Next, we explore the $\varepsilon'_{r,VO_2:Ge}(f, T)$, extract $\varepsilon'_{r,VO_2:Ge}(f, 25\,°C)$, and analyze the ac frequency and temperature-dependent conductivity, $\sigma_{ac}(f,T)$ behavior and modeling for both thin films within the 5−35 GHz frequency range below their T_c.

https://dx.doi.org/10.1021/acsaelm.0c00078
ACS Appl. Electron. Mater. XXXX, XXX, XXX−XXX

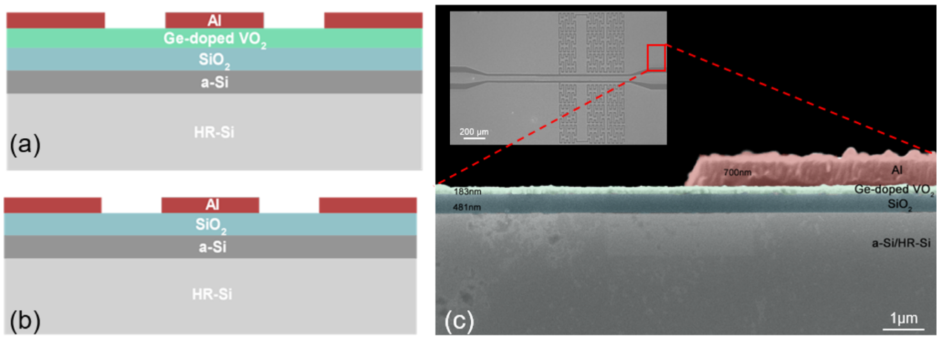

Figure 1. Cross sections of the substrate configurations used: Al depositions on (a) Ge-doped VO_2 VO_2/SiO_2/a-Si and (b) reference SiO_2/a-Si, both on high resistivity silicon substrates. (c) SEM cross-section of the PLD Ge-doped VO_2 sample, schematically shown in (a), toward the margin of the sample.

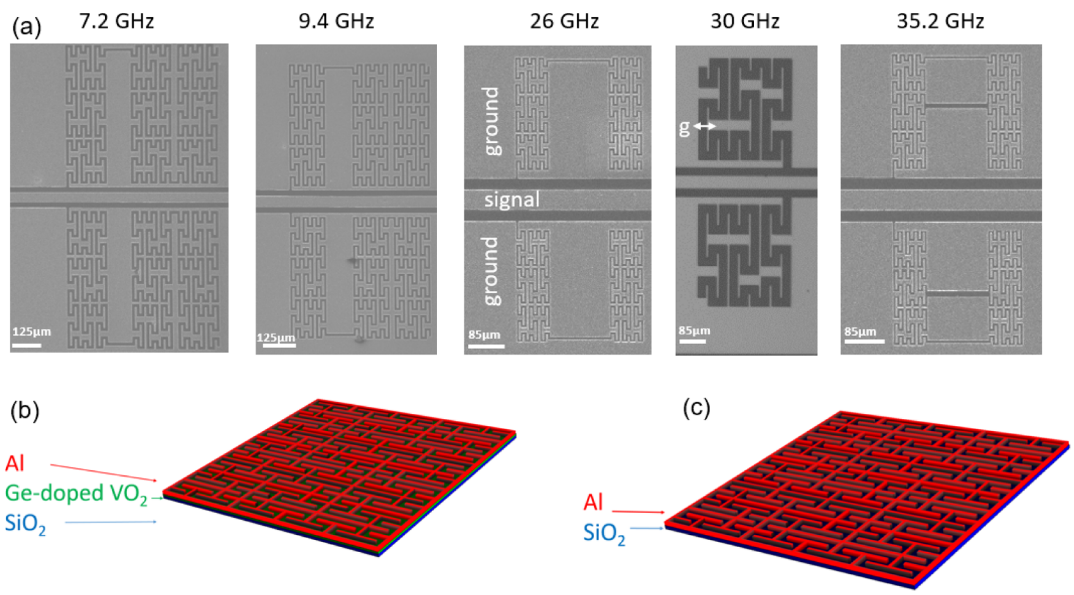

Figure 2. (a) Peano−Hilbert space-filling curve type of DGS filters fabricated for a desired resonant frequency from 7 to around 35 GHz. The designed resonance frequency, f_r shifts on (b) Ge-doped VO_2/SiO_2/a-Si/HR-Si configuration with respect to the resonances obtained on the reference substrate in (c) SiO_2/a-Si/HR-Si.

In our original procedure, we rely on the design and fabrication of a set of space-filling Peano−Hilbert curves[36] used as defected ground plane structures (DGSs)[14,37,38] in multilayer coplanar waveguide (CPW) technology. Each structure operates as a bandstop filter resonating at various frequencies within the 7−35 GHz range, depending on its (geometry and size), when on a reference substrate without the Ge-doped VO_2 thin film. The same filters fabricated on the multilayer CPW including the Ge-doped VO_2 films exhibit a relative frequency shift of their resonance frequencies (f_r) and lower bandstop attenuations. This allows us to extract $\varepsilon'_{r,VO_2:Ge}(f, T)$ and the $\sigma_{ac}(f,T)$ below T_C. The same procedure is used for undoped VO_2 thin film depositions on the same substrate configuration from the fabrication run reported in ref 16.

2. EXPERIMENTAL SECTION

2.1. Ge-Doped VO_2 Depositions. The 5% Ge-doped VO_2 film was deposited by reactive magnetron sputtering in high vacuum conditions with a base pressure in the chamber below 5×10^{-8} mbar and a process pressure of ∼7×10^{-3} mbar. The Ge is sputtered here from a V−Ge alloy target as sputtering of dopant from alloy targets is preferred over cosputtering, as previously reported,[20] because of easier process control. To deposit thermochromic VO_2 films (and avoid the formation of oxygen-poor V_2O_3 or oxygen rich, thermodynamically stable V_2O_5), the oxygen partial pressure during the process must be precisely controlled. For that, a proportional integral derivative feedback control is employed which regulates the oxygen flow based on the pressure readings of a Zirox XS22 lambda-probe oxygen sensor. Hence, the oxygen partial pressure is strictly kept in the defined narrow range ($5.8 \pm 0.2 \times 10^{-4}$ mbar). For uniform film deposition (around 200 nm in our report), the substrate is rotated at 20 rpm. The deposition temperature is 450 °C.

The 5.5% Ge-doped VO_2 was deposited with a PLD technique. The Ge-doped VO_2 film was deposited using a Solmates SMP 800 on a CMOS-compatible wafer starting from a 5.5% Ge:V_2O_5 target at a temperature of 400 °C and a laser pulse frequency of 20 Hz. The chamber was first pumped down to a base pressure of 10^{-6} mbar and then an O_2 flow of 5 sccm was employed to reach and keep the deposition pressure of 10^{-2} mbar. After deposition, the temperature was raised to 470 °C for 15 min and then the wafer was allowed to cool down, still at the same pressure, until room temperature was reached.

2.2. Ge-Doped VO_2 Characterization. The thicknesses of the Ge-doped VO_2 depositions were then determined via ellipsometry and cross-sectional SEM imaging:

The thickness of PLD-deposited Ge-doped VO_2 was determined via variable angle spectroscopic ellipsometry. The sample was

https://dx.doi.org/10.1021/acsaelm.0c00078
ACS Appl. Electron. Mater. XXXX, XXX, XXX−XXX

Table 2. Ge-Doped VO_2 and VO_2 Thin Films dc Behavior on rf CMOS Compatible Substrates

references	film type	film conductivity at 25 °C (S/m)	film conductivity at 100 °C (S/m)	IMT transition temperature (°C)	hysteresis width (°C)	$\sigma_{dc\_ON}/\sigma_{dc\_OFF}$	thickness (nm)	skin depth at 10 GHz, (μm)
12	PLD VO_2	20	64,000	68	10	3200	170	20
13	PLD VO_2	22	48,000	68	10	2181	140	23
17	5.9% Ge-doped VO_2	3.27	353	96.6	10	108	480	267
in this work	sputtered 5% Ge-doped VO_2	12.18	7633	78.2	<4.5	627	200	58
in this work	PLD 5.5% Ge-doped VO_2	55.72	145,000	74.5	<4.5	2603	243	13

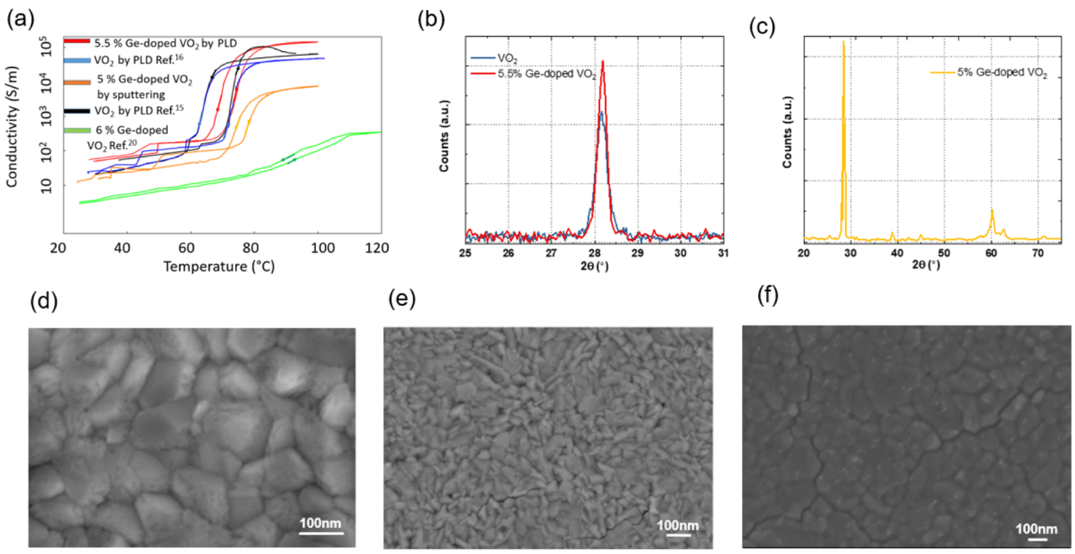

Figure 3. (a) Measured MIT/IMT transitions of the fabricated Ge-doped VO_2 films showing transition temperatures T_c at 76.2 °C for sputtered 5% Ge-doped VO_2 (orange) and at 72 °C for the PLD-deposited 5.5% Ge-doped VO_2 (red) with improved high/low conductivities and low hysteresis, compared to our previously reported[20] 5.9% Ge-doped VO_2 (in green) and undoped PLD-deposited VO_2 (in blue[16]). (b) XRD spectra of the thin films done by PLD, (c), XRD spectra of the film by sputtering. (d−f) SEM images showing the grain structure of the: sputtered Ge-doped VO_2 (d), PLD Ge-doped VO_2 (e), and the PLD undoped VO_2 corresponding to ref 16 (f).

measured at incidence angles of 65, 70, and 75° in the wavelength range from 240 to 1700 nm. The measured ellipsometric Ψ and Δ were fitted, together with the Ge-doped VO_2 layer thickness, using three independent Tauc−Lorentz oscillators. The substrate layers were measured separately on a series of reference samples to allow for an isolated measurement of the Ge-doped VO_2 properties. By this technique, the thickness of the Ge-doped VO_2 layer was determined to be 243 nm.

For the sputtered wafer, the ZEISS Supra 60VP SEM system with an electron high tension voltage of 15 kV and a working distance of ∼3 mm was used here to examine the sample cross-section shown in Figure 1c showing around 183 nm on the sample margin where the cross-section was taken.

The electrical properties of the films were studied from room temperature up to 100 °C by determining their temperature-dependent conductivity. This was done by standard four-point probe measurements using a semiconductor parameter analyzer (HP 4156C) and a control on the sample temperature up to 100 °C.

2.3. Filter Design and Electrical Characterization. The proposed methodology relies on the design and fabrication of a set of space-filling Peano−Hilbert used as curves DGSs[37,38] in multilayer (CPW). The DGS represents a small area where the ground plane metallization is removed. These structures operate as bandstop filters,[37,38] the form occupied by the DGS determining their f_r and bandstop rejection characteristics. Peano curves are space-filling curves,[36,39,40] whose lengths can be easily increased while occupying a small area. The f_r of the Peano DGS structure is dependent on their contour length, the bigger the contour length, the smaller the resonance frequency. On the other hand, the size of the width of the generating curve, g (see please Figure 2a) plays a more important role in the attenuation levels achieved. The proposed structures resonate at various frequencies within the 7 to 35 GHz range when deposited on the substrate layer configuration in Figure 1. After depositing the above described Ge-doped VO_2 layers, conventional photolithography followed by deposition of a 700 nm-thick Al layer are employed to form the CPW elements with low rf losses. The DGS are obtained by patterning the ground planes with the Peano curves. The increased length contour allows us to obtain resonances also in the lower frequency ranges of the rf spectrum, and thus, by changing their complexity and length, we can obtain several resonators covering the C, X, Ku, K, and partially the Ka bands where most wireless communications take place. The same resonators are then fabricated on the substrate layer configuration shown in Figure 1b (without the Ge-doped VO_2 thin films, whereas in (a) with it). Figure 2 presents the fabricated DGS space-filling curve structures for various resonant frequencies on the reference substrate as indicated. The ground-signal-ground distances are 24−40−24 μm for all of them, whereas the width of their generating curve (g), (schematically described in Figure 2 for one of the structures), is 10 μm for the structures resonating at 7.2 and 9.4 GHz, 5 μm for the ones at 26 and 35.2 GHz, and 21 μm for the one resonating at 30 GHz.

The scattering parameters, S, (where $S21$ is insertion and $S11$ is the return loss)[28,29] of the fabricated devices were measured with the Anritsu Vector Star Network Analyzer (VNA) in a Cascade Summit prober with controllable chuck temperature which was set to 25 °C (RT), 40, 50, and 60 °C.

https://dx.doi.org/10.1021/acsaelm.0c00078
ACS Appl. Electron. Mater. XXXX, XXX, XXX−XXX

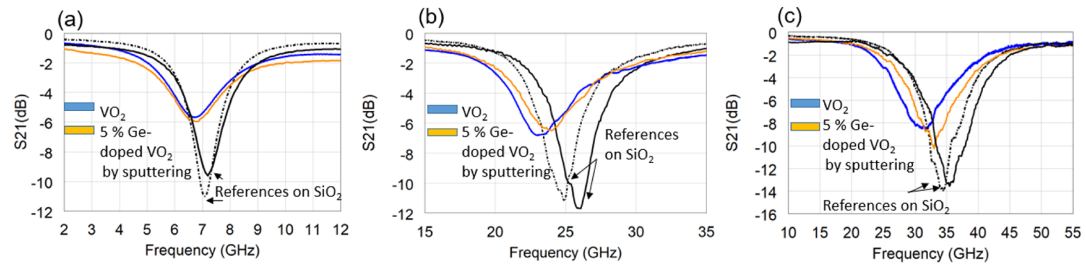

Figure 4. Room temperature measured $S21$ (dB) of fabricated Peano filters with 200 nm 5% Ge-doped VO_2 deposited by sputtering (orange) and 243 nm 5.5% Ge-doped VO_2 deposited by PLD (red). The black curve corresponds to the Peano filters on the reference substrate (on SiO_2) resonating at (a) 7.2, (b) 26, and (c) 35.2 GHz.

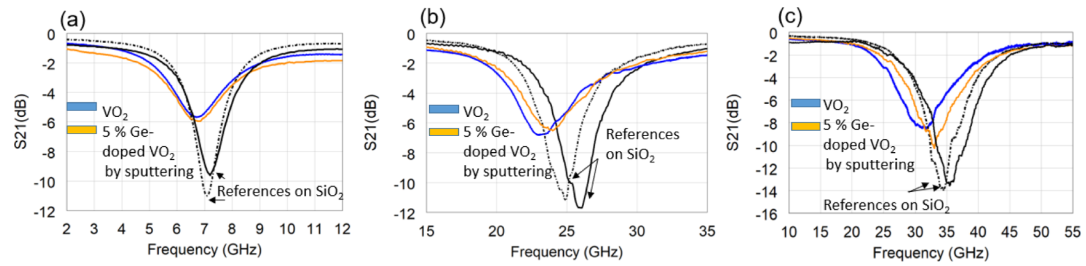

Figure 5. Room-temperature measured $S21$ (dB) of fabricated Peano filters with 200 nm 5% Ge-doped VO_2 deposited by sputtering (orange) and VO_2 from the previous run (blue).[16] The black curves correspond to the Peano filters on the reference substrates (on SiO_2 with 2400 nm metallization, dashed, whereas continuous line with 700 nm metallization) resonating at (a) 7.2 , (b) 26 , and (c) 35.2 GHz.

3. RESULTS AND DISCUSSIONS

3.1. dc Behavior at Various Temperatures. For the sputtered 5% Ge-doped VO_2, we obtained a T_c = 76.2 °C. The conductivity level at this temperature is 20 times higher as compared to our previous 5.9% Ge-doped VO_2 film work,[20] where we could report only 396 S/m at T_c = 93.6 °C. These levels are comparable with the ones obtained for VO_2 thin films with T_c = 68 °C[13−16] (Table 2), the transition temperature being slightly higher than for the other Ge-doped VO_2 films with Ge concentrations (0.1−4.3%) reported.[20]

The PLD 5.5% Ge-doped VO_2 film on the other hand shows excellent σ_{dc_ON} levels of 145,000 S/m, with a T_c of 72 °C (compared to 48,000 S/m and T_c of 68 °C in undoped VO_2 films). The dc conductivity versus temperature measurements of all films are presented in Figure 3a. In both the types of Ge-doped VO_2 films, we report an IMT−MIT (insulator to metal, metal to insulator transition) hysteresis with widths lower than 4.5 °C, far better than for undoped VO_2.

The crystallinity of the VO_2 and Ge-doped VO_2 films is confirmed by room temperature Θ−2Θ in Figure 3b and in Figure 3c by grazing incidence X-ray diffraction (Empyrean system equipped with PIXcel-1D detector, monochromatic Cu Kα radiation, grazing incidence GI angle 4°). The strongest peak at 2Θ = 27.9° in Figure 3c is assigned to the (011) diffraction peak of the monoclinic VO_2 phase according to PDF 00-044-0252. The (011) diffraction peak positions for the PLD-deposited films in Figure 3b are slightly shifted to higher angles suggesting that the presence of residual stresses the films.

The Figure 3d−f displays the SEM pictures of the continuous polycrystalline films, with larger grains (50−200 nm) in case of the sputtered Ge-doped VO_2 and the PLD undoped VO_2.

An important feature of the PLD deposition, due to its increased σ_{dc_ON}, is the skin depth[37,38] at 10 GHz which is smaller than for all previous VO_2 depositions on the same substrate. This plays an important role in the on-state conductivity of the Ge-doped VO_2, as ideally it is not desirable to operate far below the skin depth in rf-microwave design. The thin film thickness/skin depth ratio should be as big as possible,[37] else the σ_{dc_ON} values measured in dc may not be obtained while working in ac, leading to potentially bigger conductive losses.[41−43]

3.2. Room-Temperature rf Behavior. The measured $S21$ parameters of the fabricated filters on Ge-doped VO_2 (done using the layer configuration displayed in Figure 1a), and the $S21$ parameters for the reference filters (fabricated using the reference layer configuration displayed in Figure 1b) are presented in Figure 4. The three filters presented in Figure 4 resonate at 7.4 (a), 26 (b) and 35.2 (c) GHz (please see Figure 2 for their DGS layout), when fabricated on the reference substrate. The presence of the Ge-doped VO_2 film shifts down the resonance frequency of the filters while attenuating their bandstop rejection performance with respect to the ones fabricated on the reference substrate. The same trend is observed also for the other two filters (whose layouts are also presented in Figure 2) and resonating at f_r = 9.4 GHz and at f_r = 30 GHz.

In Figure 5 we show the $S21$ parameters obtained for the film used in,[16] where undoped PLD VO_2 was used with 2400 nm-thick CPW lines (unlike the 700 nm one used here for the Ge-doped VO_2 film metallization and their reference substrates), together with the $S21$ parameters for their reference filters (with 2400 nm and 700 nm-thick CPW lines). Comparing these $S21$ parameters in Figure 5 with the ones obtained on the sputtered 5% Ge-doped VO_2 thin film for the same three filters as in Figure 4 reveals a very alike behavior reflected in the very similar relative frequency shift and attenuation distortion.

3.3. Temperature- and rf-Dependent Behavior. To analyze the rf behavior of the Ge-doped VO_2 samples as a

https://dx.doi.org/10.1021/acsaelm.0c00078
ACS Appl. Electron. Mater. XXXX, XXX, XXX−XXX

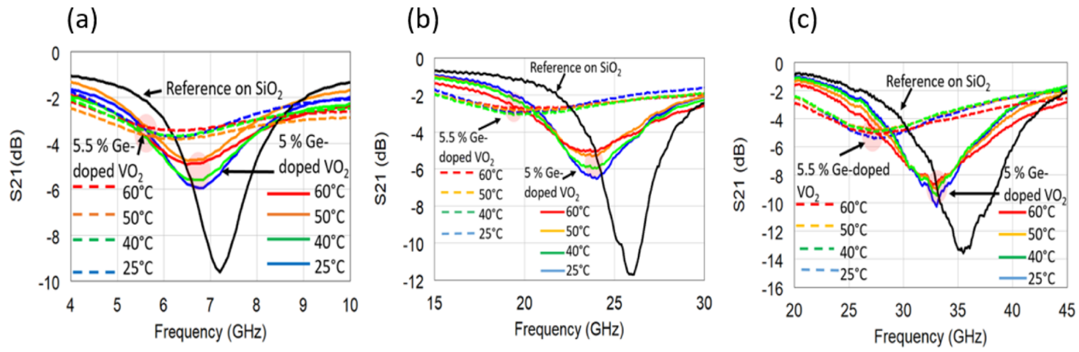

Figure 6. Measured $S21$ (dB) of the fabricated Peano filters with 200 nm 5% Ge-doped VO_2 deposited by sputtering (orange) and 243 nm 5.5% Ge-doped VO_2 deposited by PLD (red) for various temperatures. The black curve corresponds to the Peano filters on the reference substrate (on SiO_2) resonating at (a) 7.2, (b) 26, and (c) 35.2 GHz.

function of temperature, the measured transmission parameters, $S21$ of the same filters have been measured at 40, 50, and 60 °C, their performances being presented together with the $S21$ parameters of the reference filter, in Figure 6. As the temperature increases, the losses become more visible, decreasing the quality factor of the filters and their maximum bandstop attenuation around the resonance and bandpass performance elsewhere. The same trend is observed for the other fabricated structures resonating at 9.4 and 30 GHz whose layouts are presented in Figure 2.

3.4. rf Modeling and Results on Reference Substrate. Ansys HFSS simulated S21 results together with the measured (at room temperature) are shown for the structures resonating at 7.4, 26, and 35.2 GHz (on the reference substrate). The $S21$ parameters are shown in Figure 7a. Their complementary $S11$ parameters can be seen in Figure 7b–d (for the sake of simplicity only for these three structures, the same procedure being used for all). The results show a good agreement close to the resonance frequency between the simulated (designed) filters and fabricated ones for the reference layer configuration in Figure 1b, showing the very accurate modeling capabilities of Ansys HFSS when the material parameters are known. In this work, we have extracted the Ge-doped VO_2 dielectric parameters following a best-fitting procedure of an analytical model with the S parameter experimental curves (displayed in Figure 4).

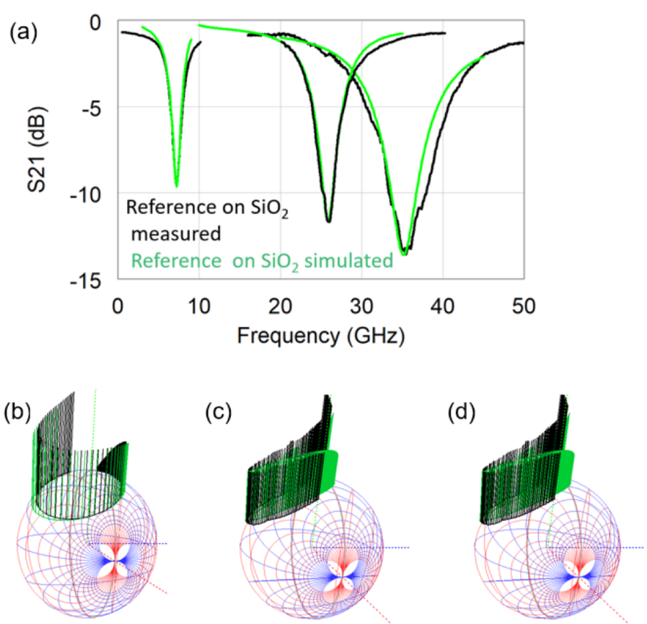

Figure 7. Room temperature measured (black) and simulated (green) with Ansys HFSS (a) $S21$ (dB) of the fabricated Peano filters on the reference substrate for f_r = 7.2 GHz one, f_r = 26 GHz, and f_r = 35.2 GHz. $S11$ on the frequency-dependent 3D Smith chart[16] for (b) f_r = 7.2 GHz, (c) f_r = 26 GHz, and (d) f_r = 35.2 GHz plotted for the same frequency range as in (a).

3.5. rf Ge-Doped VO_2 Modeling. The Ge-doped VO_2 film rf material parameters were extracted by fitting the S parameters corresponding to the measured ones around their resonance frequencies: the thin film rf material parameters were tuned around each resonance frequency leading to the experimental extraction of the dielectric constant (ε_r) and of the films below 60 °C, as already proposed in the beginning of this paper. The results are shown in Figure 8 for three of the five filters.

The de-embedding is performed around five resonance frequency points corresponding to the ones of the five Peano filters presented in Figure 2 fabricated on the two Ge-doped VO_2 thin films. The thickness of the Ge-doped VO_2 thin film is entered in the Ansys simulator according to the thin film thickness measurements on the different locations on the wafer where the filters were positioned. Additionally, this de-embedding is also done for filters fabricated on undoped VO_2 (instead of the Ge-doped VO_2) in Figure 1a from the same run as in ref 16, whose $S21$ parameters are presented in Figure 5, however using 2400 nm metallization (instead of 700 nm, corresponding to their fabrication run).

Figure 8 presents the good matching of the de-embedded results and the measured ones for the fabricated filters on the reference substrates and the two thin films.

In the extraction procedure, $\varepsilon'_{r,VO_2:Ge}(f, T = 25\ °C)$ and $\sigma_{ac}(f, T = 25\ °C)$ are optimized around each resonance frequency of the Peano filters in order to match the measured responses obtained on the PLD and sputtered Ge-doped VO_2 substrates. This is done using extensive numerical simulations and optimizations in Ansyss HFSS while extracting Ge-doped VO_2 material parameters for each deposition and frequency. The same extraction procedure is done for the undoped VO_2 thin film.

3.6. Dependence of Ge-Doped VO_2 Permittivity on Frequency. The extracted parameters, using the methodology depicted in Section 3.5, are summarized in Figures 9 and 10 at room temperature and correspond to the material parameters used in Figure 8 to fit the filter responses. The values extracted

https://dx.doi.org/10.1021/acsaelm.0c00078
ACS Appl. Electron. Mater. XXXX, XXX, XXX−XXX

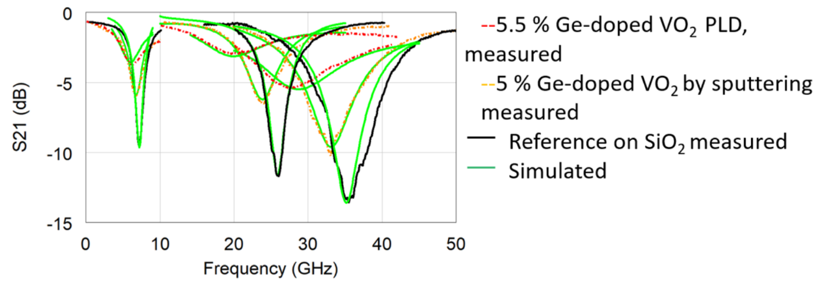

Figure 8. Room-temperature measured and simulated *S*21 parameters of three families of filters. The filters fabricated on the reference substrate (black) fit well with the designed simulated ones (green). The filters fabricated on the Ge-doped VO_2 are de-embedded and fitted on a limited frequency band (green) around their resonance frequencies for both fabricated PLD (red dotted) and sputtered (orange dotted). The fitting is done by tuning the material parameters of the (newly defined) Ge-doped VO_2 material in the Ansys HFSS. The same procedure is used for all five families of filters.

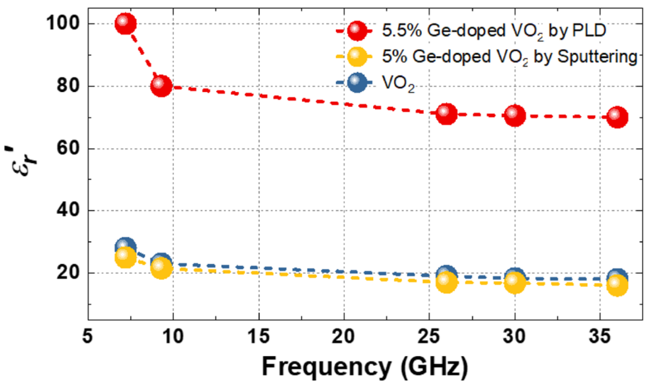

Figure 9. Room-temperature extracted dielectric constants for the Ge-doped VO_2 and (undoped PLD) VO_2 films. $\varepsilon'_{r,VO_2:Ge}$ by PLD in red. Sputtered $\varepsilon'_{r,VO_2:Ge}$ in orange. ε'_{r,VO_2} in blue.

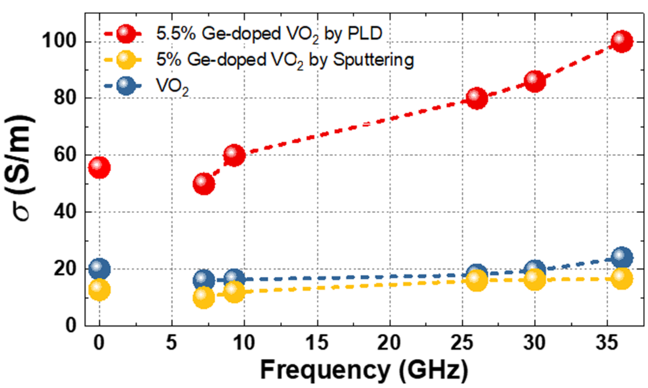

Figure 10. Room-temperature dc and extracted ac conductivity for the Ge-doped VO_2 and VO_2 thin films Ge-doped VO_2 by PLD in red. Sputtered Ge-doped VO_2 in orange. (Undoped, PLD) VO_2 thin film used in ref 16 in blue.

for the dielectric constant ($\varepsilon'_{r,VO_2:Ge}$) reflect the bigger relative frequency shift in PLD depositions. As observable also from Figure 5, the filters fabricated on the undoped VO_2 and the ones on the 5% sputtered Ge-doped VO_2 have a similar frequency shift with respect to their reference filters on SiO_2. The 5.5% PLD Ge-doped VO_2 filters on the other hand in Figure 4 show a considerably larger relative frequency shift than all their counterparts. With respect to the losses, the filters on the 5.5% PLD Ge-doped VO_2 film show decreased quality factors and bandstop performances (as already expected from the dc conductivity measurements where their measured conductivity was already 55 S/m, unlike 13 S/m for the sputtered Ge-doped VO_2 or 20 S/m for the undoped VO_2 film; Figure 3a).

On the other hand, the extracted values for the conductivity (σ_{ac_OFF}) show slightly lower values in the low-frequency range than in dc: this is partially because of the decreased room temperature when the *S* parameters were measured (lower than 25 °C). Another cause is Joule heating while measuring the values in dc, and additionally, at these frequency ranges, we work far below skin depth and although a phenomenon of decreased ac conductivity was reported in thin metal layers,[44] this may still occur for insulating thin films.

The ac conductivity values (Figure 10) are lower for the 5% sputtered Ge-doped VO_2 thin film compared to the 5.5% PLD one, while being similar to the values obtained for the undoped VO_2 film. This result is interesting and can be explained by comparing Figure 3b−d. The grain sizes of the undoped VO_2 and sputtered Ge-doped VO_2 are more similar (although dissimilar to the ones of the 5.5% PLD-deposited Ge-doped VO_2). A dependency of the THz dielectric and conductive parameters on the film's morphology was already reported for undoped VO_2 films deposited under different pressure conditions.[44] A morphology change of the films, caused by the different growth conditions of the films, brings a significant dielectric and conductivity change, detected previously in the THz regions.

Here, we observe that the undoped VO_2 and sputtered Ge-doped VO_2 have comparable grain sizes, similar dc conductivity levels and that their rf dielectric and ac conductivity levels stay similar within the 5−35 GHz frequency band too, while exhibiting a slight increase with respect to their dc values.

For the PLD Ge-doped VO_2 film, we observe a significantly different morphology and very high conductivity levels already in dc. The extracted ac conductivity shows 81% increase within the analyzed frequency band, whereas the extracted dielectric constant proves to be around 3−4 times bigger than for the other two films for a large part of the frequency spectrum. The changes in the dielectric constant might be explained by the completely different film morphology[44] and by the Kramers−Kronig relations[34] which imply that a change in the imaginary part of the permittivity (different conductivity levels) will imply a change in the real part too.

The influence of film thickness on the dielectric constant and dc conductivity was studied in the vicinity of the analyzed spectrum on sapphire substrates at 38.5 GHz and has showed little impact on them below the transition temperature.[22]

https://dx.doi.org/10.1021/acsaelm.0c00078
ACS Appl. Electron. Mater. XXXX, XXX, XXX−XXX

From an rf engineering perspective, Figures 3, 9, and 10 play an important role in the accurate and predictive design using VO_2-based films: starting with a film with low dc conductivities (below 22 S/m) and the morphology in Figure 3d,f, we can expect the films ac conductivities to stay <25 S/m below 35 GHz. Starting from a film with high conductivity levels in dc (55 S/m), we can expect 100 S/m losses at 35 GHz. This means that more care has to be taken into the design in order to face these high conductivity challenges or to be aware that the film itself may have an applicability only in the lower frequency ranges. Furthermore, starting with a film with high conductivity values in dc, we may expect a larger dielectric constant. Knowing these exact values plays an important role in estimating correctly the resonance frequencies of filters, self-resonance frequencies of rf inductors, and OFF state switches performances[4−16] overall to adapt the designs to the thin-film properties and focus on the frequency bands where the losses or dielectric changes do not critically affect the overall circuit performances.

The dielectric constant values obtained for the 5.5% PLD-deposited Ge-doped VO_2 are slightly lower than the ones reported for a VO_2 thin film on sapphire,[7] where the values are decreasing from 110 to 90 within the 5−30 GHz frequency range. The conductivity levels of the 5.5% PLD-deposited Ge-doped VO_2 show a smaller increase with frequency with respect to the conductivity levels of thin film studied on sapphire[7] whose values increase from ca. 32 to 80 S/m within the 0−30 GHz range.

The extracted dielectric constant values with our structures and models for the 5% sputtered Ge-doped VO_2 and the undoped PLD VO_2 thin film appear to be in accordance with the values reported below T_c in the W band (at 76.86 GHz), where these values do not exceed 20 for a 200 nm VO_2 thin film on Si.[45]

However, the main question is about the large difference observed between the dielectric constant of Ge-doped films deposited by PLD and by sputtering. It is worth noting that some earlier ab initio studies predicted an increase of the dielectric constant in binary oxides, driven by strain.[46] Stresses occur between neighboring grains and have been shown to affect the T_c of VO_2.[47] Such strain is sensitive to the grain size and film microstructure, and both these properties are directly influenced by the growth condition.[47] The high dielectric permittivity in PLD-deposited Ge-doped VO_2 has to be considered in conjunction with the dc conductivity, both parts of the complex dielectric response being interconnected through Kramers−Kronig relations. Within the studied frequency range (7−35 GHz), the dielectric constant of the 5.5% Ge-doped VO_2 decreases from 100 to 70 concurrently with the steady increase of the conductivity. Under the assumption of a Debye-type relaxation, these trends are consistent with the relaxation frequencies situated above the measurement range. Here, we hypothesize that the physical origin of the high dielectric constant in Ge-doped PLD-deposited films can be linked to a lattice softness associated with Ge-doping. VO_2 has a number of other phase transitions, for example M1 to metastable M2 monoclinic phases, which are likely to be affected by Ge-doping, and this may impact the dielectric response. It is also known that the energy of deposited particles in the sputtering process could be an order of magnitude higher than in PLD. Consequently, sputtered films contain a higher concentration of defects contributing to the strain relaxation, which results in a different dielectric response. Obviously, this hypothetical scenario needs more validation through further experimental studies of pure and doped VO_2 layers, strain measurements, and dielectric properties, which form a study beyond the scope of this paper. Anomalously high dc conductivity has been another feature of the Ge-doped films deposited by PLD. This effect can be attributed to the charge transport through the grain boundaries. The SEM micrographs of the PLD films reveal much smaller grains (especially for the PLD 5.5% Ge-doped VO_2) and higher density of grain boundaries compared to the sputtered films, therefore a higher grain boundary conduction is expected. A more in-depth work on the density of states[48] of Ge-doped VO_2 with various concentrations can be further foreseen to better understand this effect.

3.7. Temperature Dependence of S-Parameters of Ge-Doped VO_2 Filters. The results presented in Figure 6 for *S*21 show that as temperature increases, the quality factors of the filters decrease, meaning more losses, whereas their resonance frequency exhibits only a very slight change (due to the very slight increase of the dielectric constant).

As temperature increases, the *S*11 parameter curves become more compact while represented on a Smith chart[49] basis, while (in Figure 11 on the frequency-dependent extension of the 3D Smith chart). This can be seen in Figure 11 for the *S*11 parameters for the three filters whose *S*21 parameters were presented in Figure 6. This is a result of increased losses. The position of the *S*11 parameter curves on the 3D Smith chart is determined also by a slight mismatch due to the increased dielectric constant of the thin films. The orientation of all of them is clockwise as frequency increases and can be seen

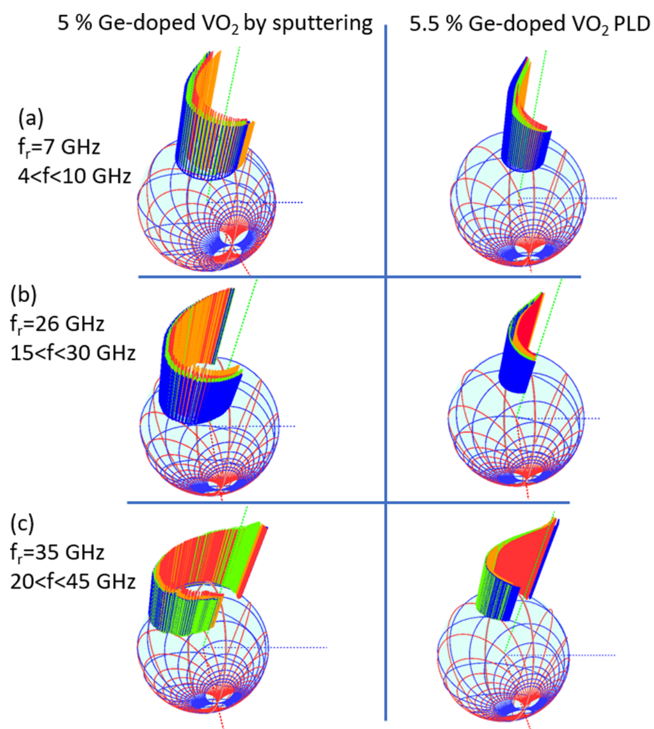

Figure 11. Reflection coefficients *S*11 on the frequency-dependent 3D Smith chart.[16] The temperature dependence of the Ge-doped VO_2 films is shown for 25 (blue), 40 (green), 50 (orange), and 60 °C (red) resonating at (a) 7.4, (b) 26 and (c) 35 GHz; (a) 4 < f < 10 GHz, (b) 15 < f < 30 GHz, (c) 20 < f < 45 GHz.

directly in this representation, unlike on a classical Smith chart or simple 3D Smith chart.

4. CONCLUSIONS

We have reported and experimentally investigated the first of their kind Ge-doped VO_2 phase change materials deposited by sputtering and PLD, with high phase change transition temperature, T_{IMT} near 80 °C and preserving excellent off- and on-state conductivities, electrically matching specifications of rf filtering. We have reported frequency (7−35 GHz) dependences of the dielectric constant and ac conductivities of thin VO_2 films via an original methodology using Peano−Hilbert filters; the extracted dielectric constant values decrease with the frequency and depend on the Ge-doping technique used. The reported dependences are extremely useful for accurately designing rf functions such as filtering. This work contributes to the field of rf reconfigurable functions with phase change materials, operating at high temperatures as per industrial requirements.

■ AUTHOR INFORMATION

Corresponding Authors

Andrei Muller − *Nanoelectronic Devices Laboratory (NanoLab), École Polytechnique Fédérale de Lausanne (EPFL), 1015 Lausanne, Switzerland*; orcid.org/0000-0002-2613-0917; Email: andrei.muller@epfl.ch

Adrian M. Ionescu − *Nanoelectronic Devices Laboratory (NanoLab), École Polytechnique Fédérale de Lausanne (EPFL), 1015 Lausanne, Switzerland*; Email: Adrian.ionescu@epfl.ch

Authors

Riyaz A. Khadar − *Powerlab, École Polytechnique Fédérale de Lausanne (EPFL), 1015 Lausanne, Switzerland*

Tobias Abel − *AMO GmbH, 52074 Aachen, Germany; Chair of Electronic Devices, RWTH Aachen University, 52062 Aachen, Germany*

Nour Negm − *AMO GmbH, 52074 Aachen, Germany; Chair of Electronic Devices, RWTH Aachen University, 52062 Aachen, Germany*

Teodor Rosca − *Nanoelectronic Devices Laboratory (NanoLab), École Polytechnique Fédérale de Lausanne (EPFL), 1015 Lausanne, Switzerland*

Anna Krammer − *Solar Energy and Building Physics Laboratory (LESO-PB), École Polytechnique Fédérale de Lausanne (EPFL), 1015 Lausanne, Switzerland*

Matteo Cavalieri − *Nanoelectronic Devices Laboratory (NanoLab), École Polytechnique Fédérale de Lausanne (EPFL), 1015 Lausanne, Switzerland*; orcid.org/0000-0001-9222-130X

Andreas Schueler − *Solar Energy and Building Physics Laboratory (LESO-PB), École Polytechnique Fédérale de Lausanne (EPFL), 1015 Lausanne, Switzerland*

Fatemeh Qaderi − *Nanoelectronic Devices Laboratory (NanoLab), École Polytechnique Fédérale de Lausanne (EPFL), 1015 Lausanne, Switzerland*

Jens Bolten − *AMO GmbH, 52074 Aachen, Germany*

Max Lemme − *AMO GmbH, 52074 Aachen, Germany; Chair of Electronic Devices, RWTH Aachen University, 52062 Aachen, Germany*; orcid.org/0000-0003-4552-2411

Igor Stolichnov − *Nanoelectronic Devices Laboratory (NanoLab), École Polytechnique Fédérale de Lausanne (EPFL), 1015 Lausanne, Switzerland*; orcid.org/0000-0003-0606-231X

Complete contact information is available at: https://pubs.acs.org/10.1021/acsaelm.0c00078

Notes

The authors declare no competing financial interest.

■ ACKNOWLEDGMENTS

This work was supported by the HORIZON 2020 FET OPEN PHASE-CHANGE SWITCH Project under Grant 737109. The authors are grateful to Yudong Cheng for help with the ellipsometry measurements at the Institute of Physics (IA) of RWTH Aachen University and to Dr. Andrey Gettikh from Cadfem GmbH for the useful conversations on HFSS parameters setup.

■ REFERENCES

(1) Zhou, Y.; Ramanathan, S. Mott Memory and Neuromorphic Devices. *Proc. IEEE* **2015**, *103*, 1289−1310.

(2) Cavalleri, A.; Dekorsy, T.; Chong, H. H. W.; Kieffer, J. C.; Schoenlein, R. W. Evidence for a Structurally-Driven Insulator-to-Metal Transition inVO2: A View from the Ultrafast Timescale. *Phys. Rev. B* **2004**, *70*, No. 161102(R).

(3) Zhou, Y.; Chen, X.; Ko, C.; Yang, Z.; Mouli, C.; Ramanathan, S. Voltage-Triggered Ultrafast Phase Transition in Vanadium Dioxide Switches. *IEEE Electron Device Lett.* **2013**, *34*, 220−222.

(4) Estes, N. J.; Chisum, D. Increased Power Handling of Vanadium Dioxide T/R Switches Using a Resonant Topology. *IEEE MTT-S International Microwave Symposium*, 2019; pp 669−672.

(5) Yang, S.; Vaseem, M.; Shamim, A. Radio-Frequency Switches: Fully Inkjet-Printed VO2-Based Radio-Frequency Switches for Flexible Reconfigurable Components. *Adv. Mater. Technol.* **2019**, *4*, 1970006.

(6) Zhang, G.; Ma, H.; Lan, C.; Gao, R.; Zhou, J. Microwave Tunable Metamaterial Based on Semiconductor-to-Metal Phase Transition. *Sci. Rep.* **2017**, *7*, 5773.

(7) Emond, N.; Hendaoui, A.; Delprat, S.; Chaker, M.; Wu, K. Theoretical and Experimental Investigation Of Thermo-Tunable Metal−Insulator−Vanadium Dioxide Coplanar Waveguide Structure. *IEEE Trans. Microwave Theory Tech.* **2017**, *65*, 1443−1455.

(8) Wang, S.; Wang, W.; Shin, E.; Quach, T.; Subramanyam, G. Tunable Inductors Using Vanadium Dioxide As The Control Material. *Microw. Opt. Technol. Lett.* **2017**, *59*, 1057−1061.

(9) Zhang, G.; Ma, H.; Lan, C.; Gao, R.; Zhou, J. Microwave Tunable Metamaterial Based on Semiconductor-to-Metal Phase Transition. *Sci. Rep.* **2017**, *7*, 5773.

(10) Vitale, W. A.; Petit, L.; Moldovan, C. F.; Fernández-Bolaños, M.; Paone, A.; Schüler, A.; Ionescu, A. M. Electrothermal Actuation of Vanadium Dioxide for Tunable Capacitors and Microwave Filters with Integrated Microheaters. *Sens. Actuators, A* **2016**, *241*, 245−253.

(11) Jiang, J.; Wong, K. W.; Mansour, R. R. A VO_2-Based 30 GHz Variable Attenuator. *2017 IEEE MTT-S International Microwave Symposium (IMS)*, 2017.

(12) Vitale, W. A. Reconfigurable Electronics Based on Metal−Insulator Transition: Steep-Slope Switches and High Frequency Functions Enabled by Vanadium Dioxide. PhD Thesis, EPFL Lausanne, 2016.

(13) Casu, E. A.; Muller, A. A.; Cavalieri, M.; Fumarola, A.; Ionescu, A. M.; Fernandez-Bolanos, M. A Reconfigurable Inductor Based On Vanadium Dioxide Insulator-To-Metal Transition. *IEEE Microw. Wireless Compon. Lett.* **2018**, *28*, 795−797.

(14) Casu, E. A.; Muller, A. A.; Fernandez-Bolanos, M.; Fumarola, A.; Krammer, A.; Schuler, A.; Ionescu, A. M. Vanadium Oxide Bandstop Tunable Filter For Ka Frequency Bands Based On A Novel Reconfigurable Spiral Shape Defected Ground Plane CPW. *IEEE Access* **2018**, *6*, 12206−12212.

(15) Muller, A. A.; Khadar, M. R.; Casu, E.; Krammer, A.; Cavalleri, M.; Zhang, J.; Schuler, A.; Ionescu, A novel reconfigurable CMOS

compatible Ka band bandstop structure using split-ring resonators and Vanadium Dioxide (VO2) phase change switches. *2019 IEEE MTT-S International Microwave Symposium Digest*, 2019; pp 865−867.

(16) Muller, A. A.; Moldoveanu, A.; Asavei, V.; Khadar, R. A.; Sanabria-Codesal, E.; Krammer, A.; Fernandez-Bolaños, M.; Cavalieri, M.; Zhang, J.; Casu, E.; Schuler, A.; Ionescu, A. M. 3D Smith Charts Scattering Parameters Frequency-Dependent Orientation Analysis and Complex-Scalar Multi-Parameter Characterization Applied to Peano Reconfigurable Vanadium Dioxide Inductors. *Sci. Rep.* **2019**, *9*, 18346.

(17) ADGM1004. https://www.analog.com/en/products/adgm1004.html (accessed Dec 2, 2019).

(18) Kovács, G. J.; Bürger, D.; Skorupa, I.; Reuther, H.; Heller, R.; Schmidt, H. Effect Of The Substrate On The Insulator−Metal Transition Of Vanadium Dioxide Films. *J. Appl. Phys.* **2011**, *109*, 063708.

(19) Lu, C.; Liang, W.; Gao, M.; Luo, S.-N.; Lin, Y. Terahertz Transmittance of Cobalt-Doped VO2 Thin Film: Investigated by Terahertz Spectroscopy and Effective Medium Theory. *IEEE Trans. Terahertz Sci. Technol.* **2019**, *9*, 177−185.

(20) Krammer, A.; Magrez, A.; Vitale, W. A.; Mocny, P.; Jeanneret, P.; Guibert, E.; Whitlow, H. J.; Ionescu, A. M.; Schüler, A. Elevated Transition Temperature in Ge Doped VO_2 Thin Films. *J. Appl. Phys.* **2017**, *122*, 045304.

(21) Prayakarao, S.; Mendoza, B.; Devine, A.; Kyaw, C.; van Dover, R. B.; Liberman, V.; Noginov, M. A. Tunable VO2/Au Hyperbolic Metamaterial. *Appl. Phys. Lett.* **2016**, *109*, 061105.

(22) Hood, P. J.; DeNatale, J. F. Millimeter-Wave Dielectric Properties Of Epitaxial Vanadium Dioxide Thin Films. *J. Appl. Phys.* **1991**, *70*, 376−381.

(23) Currie, M.; Mastro, M. A.; Wheeler, V. D. Characterizing The Tunable Refractive Index Of Vanadium Dioxide. *Opt. Mater. Express* **2017**, *7*, 1697.

(24) Verleur, H. W.; Barker, A. S.; Berglund, C. N. Optical Properties of VO_2 between 0.25 and 5 eV. *Phys. Rev.* **1968**, *172*, 788−798.

(25) Verleur, H. W. Determination of Optical Constants from Reflectance or Transmittance Measurements on Bulk Crystals or Thin Films. *J. Opt. Soc. Am.* **1968**, *58*, 1356.

(26) Chaib, A. B.; Mohammed, Z.; Zorkani, I.; Mdaa, A.; Jorio, A. Study of the Absorptance of a Thin Layer of the Vanadium Dioxide. *Indian J. Sci. Technol.* **2016**, *9*, 48.

(27) Dicken, M. J.; Aydin, K.; Pryce, I. M.; Sweatlock, L. A.; Boyd, E. M.; Walavalkar, S.; Ma, J.; Atwater, H. A. Frequency Tunable near-Infrared Metamaterials Based on VO2 Phase Transition. *Opt. Express* **2009**, *17*, 18330.

(28) Kim, B. S.; Shin, K.-Y.; Pyo, J. B.; Lee, J.; Son, J. G.; Lee, S.-S.; Park, J. H. Reversibly Stretchable, Optically Transparent Radio-Frequency Antennas Based on Wavy Ag Nanowire Networks. *ACS Appl. Mater. Interfaces* **2016**, *8*, 2582−2590.

(29) Oh, H.; Lee, S.-W.; Kim, M.; Lee, W. S.; Seong, M.; Joh, H.; Allen, M. G.; May, G. S.; Bakir, M. S.; Oh, S. J. Designing Surface Chemistry of Silver Nanocrystals for Radio Frequency Circuit Applications. *ACS Appl. Mater. Interfaces* **2018**, *10*, 37643−37650.

(30) Djordjevic, A.; Olcan, D.; Stojilovic, M.; Pavlovic, M.; Kolundzija, B.; Tosic, D. Causal Models of Electrically Large and Lossy Dielectric Bodies. *Facta Univ., Ser.: Electron. Energetics* **2014**, *27*, 221−234.

(31) Djordjevic, A. R.; Biljie, R. M.; Likar-Smiljanic, V. D.; Sarkar, T. K. Wideband Frequency-Domain Characterization of FR-4 and Time-Domain Causality. *IEEE Trans. Electromagn C.* **2001**, *43*, 662−667.

(32) Episkopou, E.; Papantonis, S.; Otter, W. J.; Lucyszyn, S. Defining Material Parameters in Commercial EM Solvers for Arbitrary Metal-Based THz Structures. *IEEE Trans. Terahertz Sci. Technol.* **2012**, *2*, 513−524.

(33) Ansys HFSS v. 17.2 helpfile.

(34) Seier, P. S. Dielectric Material Characterization up to Terahertz Frequencies Using Planar Transmission Lines. PhD Thesis, Technische Universität Dresden, 2019.

(35) Psarras, G. C.; Manolakaki, E.; Tsangaris, G. M. Dielectric Dispersion and Ac Conductivity in—Iron Particles Loaded—Polymer Composites. *Composites, Part A* **2003**, *34*, 1187−1198.

(36) Glaeser, G.; Polthier, K. *Images of Pure Mathematics*; Springer Spectum: Heidelberg, 2010.

(37) Simons, R. *Coplanar Waveguide Circuits, Components, and Systems*; John Wiley: New York, 2001.

(38) Safwat, A. M. E.; Podevin, F.; Ferrari, P.; Vilcot, A. Tunable Bandstop Defected Ground Structure Resonator Using Reconfigurable Dumbbell-Shaped Coplanar Waveguide. *IEEE Trans. Microwave Theory Tech.* **2006**, *54*, 3559−3564.

(39) El-Khouly, E.; Ghali, H.; Khamis, S. A. High Directivity Antenna Using A Modified Peano Space-Filling Curve. *IEEE Antenn. Wireless Propag. Lett.* **2007**, *6*, 405−407.

(40) Mandelbrot, B. *The Fractal Geometry of Nature*; W.H. Freeman: New York, 1983.

(41) Laman, N.; Grischkowsky, D. Terahertz Conductivity of Thin Metal Films. *Appl. Phys. Lett.* **2008**, *93*, 051105.

(42) Seo, M.; Kyoung, J.; Park, H.; Koo, S.; Kim, H.-S.; Bernien, H.; Kim, B. J.; Choe, J. H.; Ahn, Y. H.; Kim, H.-T.; Park, N.; Park, Q.-H.; Ahn, K.; Kim, D.-S. Active Terahertz Nanoantennas Based on VO_2 Phase Transition. *Nano Lett.* **2010**, *10*, 2064−2068.

(43) Krupka, J.; Derzakowski, K.; Zychowicz, T.; Givot, B. L.; Egbert, W. C.; David, M. M. Measurements of the Surface Resistance and Conductivity of Thin Conductive Films at Frequency about 1GHz Employing Dielectric Resonator Technique. *J. Eur. Ceram. Soc.* **2007**, *27*, 2823−2826.

(44) Luo, Y. Y.; Su, F. H.; Pan, S. S.; Xu, S. C.; Zhang, C.; Pan, J.; Dai, J. M.; Li, P.; Li, G. H. Terahertz Conductivities of VO2 Thin Films Grown under Different Sputtering Gas Pressures. *J. Alloys Compd.* **2016**, *655*, 442−447.

(45) Hashemi, M. R. M.; Berry, C. W.; Merced, E.; Sepúlveda, N.; Jarrahi, M. Direct Measurement of Vanadium Dioxide Dielectric Properties in W-Band. *J. Infrared, Millim. Terahertz Waves* **2014**, *35*, 486−492.

(46) Bousquet, E.; Spaldin, N. A.; Ghosez, P. Strain-Induced Ferroelectricity in Simple Rocksalt Binary Oxides. *Phys. Rev. Lett.* **2010**, *104*, 037601.

(47) Huffman, T. J.; Xu, P.; Hollingshad, A. J.; Qazilbash, M. M.; Wang, L.; Lukaszew, R. A.; Kittiwatanakul, S.; Lu, J.; Wolf, S. A. Modification of Electronic Structure in Compressively Strained Vanadium Dioxide Films. *Phys. Rev. B* **2015**, *91*, 205140.

(48) Lu, H.; Robertson, J. Density Functional Theory Studies of the Metal−Insulator Transition in Vanadium Dioxide Alloys. *Phys. Status Solidi B* **2019**, *256*, 1900210.

(49) Wang, Z.; Uzlu, B.; Shaygan, M.; Otto, M.; Ribeiro, M.; Marín, E. G.; Iannaccone, G.; Fiori, G.; Elsayed, M. S.; Negra, R.; Neumaier, D. Flexible One-Dimensional Metal−Insulator−Graphene Diode. *ACS Appl. Electron. Mater.* **2019**, *1*, 945−950.

https://dx.doi.org/10.1021/acsaelm.0c00078
ACS Appl. Electron. Mater. XXXX, XXX, XXX−XXX